Tensor-Factorization-Based 3D Single Image Super-Resolution with Semi-Blind Point Spread Function Estimation

Janka Hatvani, Adrian Basarab, Jérôme Michetti, Miklós Gyöngy, Denis Kouamé, Janka Hatvani

TENSOR-FACTORIZATION-BASED 3D SINGLE IMAGE SUPER-RESOLUTION WITH SEMI-BLIND POINT SPREAD FUNCTION ESTIMATION

J. Hatvani[⋆†] *A. Basarab*[†] *J. Michetti* [†] *M. Gyöngy* [⋆] *D. Kouamé* [†]

[⋆] Pázmány Péter Catholic Unviersity
Faculty of Information Technology and Bionics
50/a Práter utca, H-1083 Budapest

[†]Université Paul Sabatier Toulouse 3
Institute de Recherche en Informatique de Toulouse
118 r. de Narbonne, F-31062 Toulouse

ABSTRACT

A volumetric non-blind single image super-resolution technique using tensor factorization has been recently introduced by our group. That method allowed a 2-order-of-magnitude faster high-resolution image reconstruction with equivalent image quality compared to state-of-the-art algorithms. In this work a joint alternating recovery of the high-resolution image and of the unknown point spread function parameters is proposed. The method is evaluated on dental computed tomography images. The algorithm was compared to an existing 3D super-resolution method using low-rank and total variation regularization, combined with the same alternating PSF-optimization. The two algorithms have shown similar improvement in PSNR, but our method converged roughly 40 times faster, under 6 minutes both in simulation and on experimental dental computed tomography data.

Index Terms— image enhancement, 3D super-resolution, semi-blind deconvolution, 3D computed tomography

1. INTRODUCTION

Super-resolution algorithms attempt to enhance the image quality in terms of resolution either by modifications of the hardware or as a post-processing algorithmic step. In this paper the latter group of methods is investigated, noted as SR. Such algorithms either use a sequence of low-resolution (LR) images [1], scenes of different modalities [2], or a single image (SISR) [3] to provide an estimation of their high-resolution (HR) counterpart. It is usually assumed that the LR image is the blurred and decimated version with some additive noise of the HR image. This model allows the formulation of an ill-posed inverse problem, which requires suitable regularization for obtaining a stable solution. State-of-the-art techniques use regularizers like total variation [4], low rank [5], wavelet [6] or patch-based structural similarity constraint [7]. Convolutional neural networks have also been trained to map the LR image to its HR counterpart with success [8–11], but require large training databases which are not always easy to obtain in practice, and are limited to the application they were trained for. However, for 3D images the above methods are not applicable either because they are not implemented for higher dimensions, or they suffer from heavy computational cost.

Tensor factorization had been applied previously for hyperspectral – multispectral image fusion in [12]. In our previous paper [13] this technique was applied for the SISR task. In that method canonical polyadic decomposition (CPD) is carried out on the 3D image, which can be thought of as a sum of rank-1 tensors. As the image is not unfolded into a 2D matrix, local information of neighbouring pixels is maintained.

In this paper, the issue of the system point spread function (PSF) is addressed. In our previous work the PSF was estimated directly from the data knowing the LR-HR image pairs [13]. Herein, a joint recovery of the PSF and the HR image is proposed, assuming that the image blur is caused by a Gaussian kernel, and its standard deviation is within a predefined interval. The HR image and the parameters of the Gaussian kernel are updated alternately in an iterative manner. The proposed method was evaluated on dental computed tomography (CT) images, both on simulated and real data. The results are compared to a method using a recent 3D SISR technique for the estimation of the HR image with low-rank and total-variation regularization (denoted as LRTV). The Gaussian parameters are updated as in the proposed method, alternating between the two estimation steps.

The rest of this paper is organized as follows: first the relevant tensor algebra is summarized in Section 2. In Section 3, the image degradation problem is formulated, followed by the description of the image and kernel estimation steps. In Section 4, the test environment is introduced, and the results are compared through qualitative and quantitative measures. The algorithms achieve similar enhancement of the LR images, but the proposed method executes an order of magnitude

This research has been partially supported by the European Union, co-financed by the European Social Fund (EFOP-3.6.3-VEKOP- 16-2017-00002 and by Pázmány University KAP17-19.

This work was funded by the thematic trimester on image processing of the CIMI Labex, Toulouse, France, with the Program ANR-11-IDEX-0002-02 under Grant ANR-11-LABX-0040-CIMI

faster and its parameter tuning is also easier.

2. TENSOR OPERATIONS

In this section, operations from tensor algebra necessary for the proposed method are summarized. Readers may refer to [12–14] for further details.

A 3D image volume is a third-order tensor $\boldsymbol{X} \in \mathbb{R}^{I\times J\times K}$. Its mode-1 fibers (columns) are the $\boldsymbol{X}(:,j,k)$ vectors, the mode-2 fibers (rows) are $\boldsymbol{X}(i,:,k)$, and the mode-3 fibers are $\boldsymbol{X}(i,j,:)$. The outer product ($u^1 \circ u^2 \circ u^3$) between one mode-1 (u^1), one mode-2 (u^2) and one mode-3 array (u^3) is a rank-1 third order tensor.

The smallest number (F) of rank-1 tensors building up tensor $\boldsymbol{X}$ is called the tensor rank of $\boldsymbol{X}$. The resulting factorization of $\boldsymbol{X}$ is called the CPD of $\boldsymbol{X}$ given by

$$\boldsymbol{X} = [\![U^1, U^2, U^3]\!] = \sum_{f=1}^{F} U^1(:,f) \circ U^2(:,f) \circ U^3(:,f) \tag{1}$$

where $\overline{U} = \{U^1, U^2, U^3\}$ is a set of three 2D matrices, $\{U^1 \in \mathbb{R}^{I\times F}, U^2 \in \mathbb{R}^{J\times F}, U^3 \in \mathbb{R}^{K\times F}\}$, known as the decomposition of the tensor $\boldsymbol{X}$.

The CPD is essentially unique (allowing permutations within U^1, U^2, U^3), making $\overline{U}$ identifiable almost surely if $F \leq 2^{\lfloor log_2 J\rfloor + \lfloor log_2 K\rfloor - 2}$ [15]. This condition allows identifiability even for large tensor ranks (a matrix of $300\times300\times300$ might have $F \leq 2^{14} = 16384$).

Multiplication between a 2D matrix and a 3D tensor along dimension n is the mode-n product (denoted with $\times_n$). The mode-n fibers of a tensor are extracted and are pre-multiplied by the 2D matrix. Along the first dimension it corresponds to

$$\begin{aligned} \boldsymbol{X}\times_1(P_1 \in \mathbb{R}^{I^*\times I}) &= (\boldsymbol{X_1} \in \mathbb{R}^{I^*\times J\times K}) \\ \text{where } \boldsymbol{X_1}(:,j,k) &= P_1\boldsymbol{X}(:,j,k) \end{aligned} \tag{2}$$

where I^* is an arbitrary integer number. The mode-n products along the other two dimensions can be calculated analogously. Using (1) the mode-n products can also be expressed as

$$\boldsymbol{X} \times_1 P_1 \times_2 P_2 \times_3 P_3 = [\![P_1U^1, P_2U^2, P_3U^3]\!]. \tag{3}$$

The matricization (unfolding) of the tensor $\boldsymbol{X}$ from 3D to 2D can be realized along any of the three dimensions again. In the mode-*n* matricization the mode-*n* fibers form the columns of $\boldsymbol{X}^{(n)}$ in lexicographical order. Along the first dimension it is written as

$$\begin{aligned} (\boldsymbol{X}^{(1)} \in \mathbb{R}^{I\times JK}) = [&\boldsymbol{X}(:,1,1), \boldsymbol{X}(:,2,1), ...\boldsymbol{X}(:,J,1), \\ &\boldsymbol{X}(:,1,2), \boldsymbol{X}(:,2,2)..., \boldsymbol{X}(:,J,K)] \end{aligned} \tag{4}$$

and can be calculated analogously for the other 2 dimensions. Using $\overline{U}$ of $\boldsymbol{X}$ it can be written as

$$\boldsymbol{X}^{(1)} = U^1(U^3 \odot U^2)^T \tag{5}$$

where $\odot$ is the Kathri-Rao product [13].

3. METHODS

3.1. Problem formulation

The classical image degradation model of SISR defines the LR image ($\boldsymbol{Y} \in \mathbb{R}^{I/r_1\times J/r_2\times K/r_3}$) as a downsampled (with rate $r_1 = r_2 = r_3 = r$ in our application) and blurred (with kernel h) HR image ($\boldsymbol{X} \in \mathbb{R}^{I\times J\times K}$) with some additive Gaussian white noise ($\mathbf{N} \in \mathbb{R}^{I/r_1\times J/r_2\times K/r_3}$). Herein, the PSF is considered Gaussian, a common assumption in many applications. This can be expressed as

$$\text{vec}(\boldsymbol{Y}) = DH\text{vec}(\boldsymbol{X}) + \text{vec}(\boldsymbol{N}) \tag{6}$$

where vec$(\cdot)$ vectorizes the tensor elements in lexicographical order. $H \in \mathbb{R}^{IJK\times IJK}$ is the block-circulant form of the 3D Gaussian kernel h. A 3D Gaussian kernel h of standard deviations $\overline{\sigma} = [\sigma_1, \sigma_2, \sigma_3]$ can be decomposed as $h = h_1 \circ h_2 \circ h_3$, based on its separability. The corresponding block-circulant matrices using zero-padding and circular shift are $H_1 \in \mathbb{R}^{I\times I}, H_2 \in \mathbb{R}^{J\times J}, H_3 \in \mathbb{R}^{K\times K}$. The downsampling operator averages blocks of r neighboring pixels. In matrix form these are $D_1 \in \mathbb{R}^{I/r\times I}, D_2 \in \mathbb{R}^{J/r\times J}, D_3 \in \mathbb{R}^{K/r\times K}$.

Let $\overline{U} = \{U^1 \in \mathbb{R}^{I\times F}, U^2 \in \mathbb{R}^{J\times F}, U^3 \in \mathbb{R}^{K\times F}\}$ be the CPD of HR tensor $\boldsymbol{X}$. Using (3) and the separated kernels, (6) can be written as

$$\begin{aligned} \boldsymbol{Y} &= \boldsymbol{X} \times_1 D_1H_1 \times_2 D_2H_2 \times_3 D_3H_3 + \boldsymbol{N} \\ &= [\![D_1H_1U^1, D_2H_2U^2, D_3H_3U^3]\!] + \boldsymbol{N}. \end{aligned} \tag{7}$$

The semi-blind SISR task is now to find the set of matrices $\overline{U}$ and the parameter $\overline{\sigma}$ which minimizes

$$\min_{\overline{U},\overline{\sigma}} \left\| \boldsymbol{Y} - [\![D_1H_1(\sigma_1)U^1, D_2H_2(\sigma_2)U^2, D_3H_3(\sigma_3)U^3]\!] \right\|_F^2 \tag{8}$$

where $\|\cdot\|_F$ denotes the Frobenius norm (square root of the sum of the squared matrix elements).

As problem (8) is non-convex, an alternating optimization method is proposed, minimizing (8) for U^1, U^2, U^3 and $\sigma_1, \sigma_2, \sigma_3$, respectively.

3.2. Image estimation

The image estimation step is calculated as described in [13]. When minimizing over U_n, the tensors are mode-*n*-matricized using (4) and (5) giving

$$\begin{aligned} &\min_{U^1} \frac{1}{2} \left\| \boldsymbol{Y}^{(1)} - D_1H_1U^1(D_3H_3U^3 \odot D_2H_2U^2)^T \right\|_F^2 \\ &\min_{U^2} \frac{1}{2} \left\| \boldsymbol{Y}^{(2)} - D_2H_2U^2(D_3H_3U^3 \odot D_1H_1U^1)^T \right\|_F^2 \\ &\min_{U^3} \frac{1}{2} \left\| \boldsymbol{Y}^{(3)} - D_3H_3U^3(D_2H_2U^2 \odot D_1H_1U^1)^T \right\|_F^2. \end{aligned} \tag{9}$$

The least-square estimator of (9) obtained with the Moore-Penrose pseudo-inverse ($^+$) and Tikhonov regularization is

$$\begin{aligned} U^1 &= (D_1H_1)^+\boldsymbol{Y}^{(1)}(D_3H_3U^3 \odot D_2H_2U^2)^{+T} \\ U^2 &= (D_2H_2)^+\boldsymbol{Y}^{(2)}(D_3H_3U^3 \odot D_1H_1U^1)^{+T} \\ U^3 &= (D_3H_3)^+\boldsymbol{Y}^{(3)}(D_2H_2U^2 \odot D_1H_1U^1)^{+T} \end{aligned} \tag{10}$$

3.3. PSF estimation

The PSF estimation was implemented based on [16]. As H is a block circulant with circulant blocks (BCCB) matrix, $H\text{vec}(\mathbf{X})$ of (6) can be rewritten using the Fourier transform $\mathcal{F}$ as

$$H\text{vec}(\mathbf{X}) = \mathcal{F}^{-1}(\mathcal{F}\tilde{h} \cdot \mathcal{F}\mathbf{X}) \tag{11}$$

where $\tilde{h}$ is the zero-padded, circularly shifted version of kernel h and the operation $(\cdot)$ is the element-wise matrix multiplication (Hadamard product). This formulation radically reduces the size of the matrices to be multiplied. The kernel $\tilde{h}$ can be expressed as

$$\tilde{h}(\overline{\sigma}) = \frac{1}{\sigma_1\sigma_2\sigma_3\sqrt{2\pi}^3} e^{\frac{1}{2}\left(\frac{x^2}{\sigma_1} + \frac{y^2}{\sigma_2} + \frac{z^2}{\sigma_3}\right)}, \tag{12}$$

where x, y, z are the fixed 3D evaluation coordinates of the zero-padded, shifted kernel. It can be assumed, based on prior knowledge depending on the application, that all elements of $\overline{\sigma}$ are within a given interval denoted by a_1, a_2, and a_3 respectively. This is characterized by the indicator functions $i(\overline{\sigma}) = i(\sigma_1) + i(\sigma_2) + i(\sigma_3)$. Combining this with (11) and (12) the kernel optimization problem can now be written as

$$\begin{aligned} &\min_{\overline{\sigma}} \left\| \boldsymbol{Y} - \mathcal{F}^{-1}(\mathcal{F}\tilde{h}(\overline{\sigma}) \cdot \mathcal{F}\mathbf{X}) \right\|_F^2 + i(\overline{\sigma}) \\ &\quad = \min_{\overline{\sigma}} G(\overline{\sigma}) + i(\overline{\sigma}) \end{aligned} \tag{13}$$

Knowing that the solution of the proximal operator for the above problem is a projection ($\prod$) onto the corresponding a_1, a_2, a_3 intervals, the solution of (13) will be the fixed point of

$$\overline{\sigma} = \prod \left(\overline{\sigma} - \gamma \frac{dG(\overline{\sigma})}{d\overline{\sigma}} \right), \tag{14}$$

where γ, the step size is a small enough coefficient (its value might be changed at each iteration). In (14) the data fidelity term $G(\overline{\sigma})$ is estimated with a gradient descent step and the indicator function is taking effect through the projection operator.

The algorithm was implemented in Matlab 2017, and for the basic tensor operations and the tensor structure the TensorLab toolbox was employed [17]. The image and kernel estimation steps were joined in our tensor-factorization-based SISR algorithm [1] with semi-blind PSF estimation (TF-SISR-blind) as shown in Algorithm 1.

[1]The Matlab code corresponding to [13] is available at https://www.irit.fr/ Adrian.Basarab/codes.html

Algorithm 1 TF-SISR algorithm

Input: $\boldsymbol{Y}, F, a_1, a_2, a_3, \overline{\sigma}_0, r, N, M, \epsilon$

Initialize $\overline{U}$ with normally distributed values
$D_1, D_2, D_3 \leftarrow$ decimation operator with a factor r
for i = 0:N **do**
  $H_1, H_2, H_3 \leftarrow$ Gaussian kernels of $\overline{\sigma}_i$
  for j = 0:M **do**
    $U^1 \leftarrow Y^{(1)}, U^2, U^3$
    $U^2 \leftarrow Y^{(2)}, U^1, U^3$ ▷ update using (10)
    $U^3 \leftarrow Y^{(3)}, U^1, U^2$
  end for
  $\hat{\mathbf{X}} \leftarrow \overline{U}$ ▷ build using (1)
  Initialize diff$= inf$
  while diff $> \epsilon$ **do**
    $\overline{\sigma}^{i+1} \leftarrow \overline{\sigma}^i, \hat{\mathbf{X}}$ ▷ update using (14)
    diff = max$(\overline{\sigma}^{i+1} - \overline{\sigma}^i)$
  end while
end for

Output: $\boldsymbol{X}$, the estimated high resolution image

4. RESULTS AND DISCUSSION

4.1. Simulated and experimental data

The algorithm was evaluated on dental CT images. The HR images were recorded with a QuantumFX micro-CT system from Perkin Elmer (resolution 1 LP/mm at 50% MTF, meaning that spatial frequencies of 1 line pair per mm are depicted at 50% of the modulation transfer function) and their LR counterparts with a Carestream 81003D limited cone-beam CT system (CBCT, resolution 10 LP/mm at 50% MTF, 10 times lower than that of the micro-CT). Further details on the data acquisition are introduced in [11]. Within the simulation the LR images were obtained by blurring and down-sampling the micro-CT images (considered as the ground truth in CT imaging) without added noise, with parameters listed in Table 1. In the experimental setting, the LR input was the CBCT volume.

The proposed method was compared with the LRTV method described in [5]. Within this 3D SISR problem is solved by the alternating direction method of multipliers (ADMM), minimizing the sum between a quadratic data fidelity term and two law rank and total variation regularizers. The original code was combined with the PSF estimation step of (14). The method is further denoted as LRTV-blind.

The TF-SISR-blind algorithm ran 3 overall iterations ($N = 3$), 5 image-update iterations in each loop ($M = 5$), and the kernel update repeated until converged. The initial step size γ was set to 1e-5 and decreased linearly in the outer loop. The parameter setting for the simulation and experimental data is listed in Table 1.

The LRTV-blind algorithm ran 3 overall iterations, in each loop running 3 LRTV iterations for image update, followed by

Table 1. Test parameters and results

	Simulation	Experiment
HR pixel number	287×266×392	274×278×474
chosen F	400	
downsampling rate r	2	
ground truth $\overline{\sigma}$	[6.0 6.0 6.0]	–
initialized $\overline{\sigma}$	[8.0 8.0 7.0]	[8.0 8.0 7.0]
$\overline{\sigma}$ with LRTV-blind	[4.7 4.6 6.3]	[7.6 6.5 7.4]
$\overline{\sigma}$ with TF-SISR-blind	[5.0 4.9 4.8]	[8.5 7.8 6.5]
LR–HR PSNR	22.32 dB	19.42 dB
LRTV-blind PSNR	24.39 dB	25.63 dB
TF-SISR-blind PSNR	26.53 dB	30.07 dB
LRTV-blind time	9087 s	11823 s
TF-SISR-blind time	298 s	354 s

Gaussian parameter optimization until convergence. The hyperparameters controlling the regularization were set to 0.07 for the low-rank and 0.02 for total variation.

Note that for both methods, all the hyperparameters were manually tuned to provide the best results possible in terms of visual inspection. In both methods the initialization of $\overline{\sigma}$ is started from the values listed in Table 1, and the a_1, a_2, a_3 intervals of the projections are set corresponding to the initialized $\overline{\sigma}$ as $[\overline{\sigma}-4, \overline{\sigma}+2]$. For the experimental data no ground truth value of the Gaussian parameters was available.

The enhancement was measured quantitatively through the peak signal-to-noise ratio (PSNR) [18] between the ground truth micro-CT and the LR, TF-SISR-blind, LRTV-blind images respectively.

4.2. Super-resolution results

The results are illustrated through one slice extracted from the volumes in Fig. 1. It can be seen that with LRTV-blind the image is contrasted, smoothed and the root canal (dark region inside the tooth) is more dilated as a result of the TV regularization, both in the simulation and on the experimental data. Note that no such parameters need to be tuned in TF-SISR-blind, resulting in more natural images.

In Table 1 the quantitative results are listed. In simulation the PSNR improved by 18.9% in TF-SISR and 9.3% in LRTV, while on the experimental data by 54.8% and 31.9% respectively. It can be seen that the Gaussian parameters of the simulation converged to a lower value than used for blurring, because of the non-convex nature of the problem. However, the most important improvement of TF-SISR-blind remains its runtime, being roughly 40 times faster compared to the LRTV-blind on a standard PC with an Intel® Core™ i7 22.5GHz processor and 16 GB of RAM.

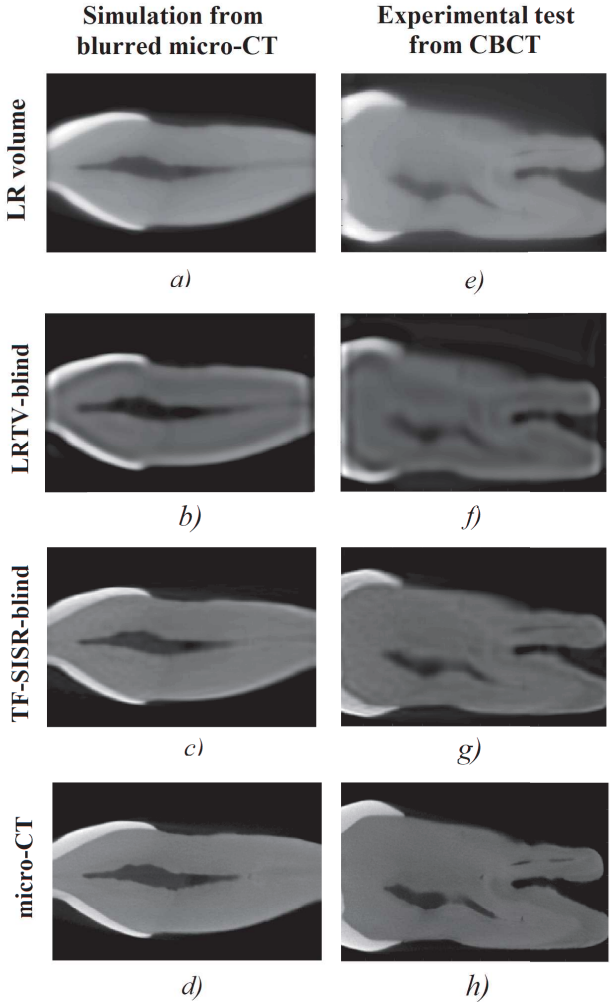

Fig. 1. Image enhancement. On the left slices corresponding to the simulation, on the right the slices from the experimental volume can be seen. A coronal slice was chosen for demonstration. The LR images are shown on the scale of the HR images using linear interpolation.

5. CONCLUSION

In this paper a fast method for single image super-resolution with joint Gaussian kernel estimation was introduced. The algorithm managed to improve the image quality similarly to an existing ADMM reconstruction method using low-rank and total-variation regularization. The main advantage of the algorithm is its speed, processing 3D volumes in less than 5 minutes with standard Matlab implementation on a desktop computer. In future work the effect of embedding classical priors into the tensor-based model will be investigated on different image classes.

6. REFERENCES

[1] Sina Farsiu, M Dirk Robinson, Michael Elad, and Peyman Milanfar, "Fast and robust multiframe super resolution," *IEEE Trans. Image Process.*, vol. 13, no. 10, pp. 1327–1344, 2004.

[2] Haitao Yin, Shutao Li, and Leyuan Fang, "Simultaneous image fusion and super-resolution using sparse representation," *Information Fusion*, vol. 14, no. 3, pp. 229–240, 2013.

[3] Kwang In Kim and Younghee Kwon, "Single-image super-resolution using sparse regression and natural image prior," *IEEE Trans. Pattern Anal. Mach. Intell.*, vol. 32, no. 6, pp. 1127–1133, 2010.

[4] Alina Toma, Loïc Denis, Bruno Sixou, Jean-Baptiste Pialat, and Françoise Peyrin, "Total variation super-resolution for 3D trabecular bone micro-structure segmentation," in *Proc. 22nd European Signal Processing Conference (EUSIPCO)*, Lisbon, Portugal, Sept. 2014, pp. 2220–2224.

[5] Feng Shi, Jian Cheng, Li Wang, Pew-Thian Yap, and Dinggang Shen, "LRTV: MR image super-resolution with low-rank and total variation regularizations," *IEEE Trans. Med. Imag.*, vol. 34, no. 12, pp. 2459–2466, 2015.

[6] Wenkun Zhang, Hanming Zhang, Linyuan Wang, Ailong Cai, Lei Li, and Bin Yan, "Limited angle CT reconstruction by simultaneous spatial and radon domain regularization based on TV and data-driven tight frame," *Nuclear Instruments and Methods in Physics Research Section A: Accelerators, Spectrometers, Detectors and Associated Equipment*, vol. 880, pp. 107–117, 2018.

[7] José V Manjón, Pierrick Coupé, Antonio Buades, Vladimir Fonov, D Louis Collins, and Montserrat Robles, "Non-local MRI upsampling," *Medical image analysis*, vol. 14, no. 6, pp. 784–792, 2010.

[8] Ozan Oktay, Wenjia Bai, Matthew Lee, Ricardo Guerrero, Konstantinos Kamnitsas, Jose Caballero, Antonio de Marvao, Stuart Cook, Declan ORegan, and Daniel Rueckert, ," in *Proc. 19th MICCAI Int. Conf.*, Athens, Greece, Oct.17–21 2016, Springer, pp. 246–254.

[9] Sevim Cengiz, Maria del C Valdes-Hernandez, and Esin Ozturk-Isik, "Super resolution convolutional neural networks for increasing spatial resolution of ^{1}h magnetic resonance spectroscopic imaging," in *Proc. 21st MIUA Annu. Conf.*, Edinburgh, UK, July11-13 2017, Springer, pp. 641–650.

[10] YiNan Zhang and MingQiang An, "Deep learning- and transfer learning-based super resolution reconstruction from single medical image," *J. Healthc. Eng.*, vol. 2017, Art. ID 5859727, 20 pages, 2017.

[11] Janka Hatvani, András Horváth, Jérome Michetti, Adrian Basarab, Denis Kouamé, and Miklós Gyöngy, "Deep learning-based super-resolution applied to dental computed tomography," *IEEE Transactions on Radiation and Plasma Medical Sciences*, pp. 1–1, 2018, In Press.

[12] C. I. Kanatsoulis, X. Fu, N. D. Sidiropoulos, and W. Ma, "Hyperspectral super-resolution: A coupled tensor factorization approach," *IEEE Trans. Signal Process.*, vol. 66, no. 24, pp. 6503–6517, Dec 2018.

[13] Janka Hatvani, Adrian Basarab, Jean-Yves Tourneret, Miklós Gyöngy, and Denis Kouamé, "A tensor factorization method for 3d super-resolution with application to dental ct," *IEEE transactions on medical imaging*, 2018, In Press.

[14] Tamara G Kolda and Brett W Bader, "Tensor decompositions and applications," *SIAM review*, vol. 51, no. 3, pp. 455–500, 2009.

[15] Luca Chiantini and Giorgio Ottaviani, "On generic identifiability of 3-tensors of small rank," *SIAM Journal on Matrix Analysis and Applications*, vol. 33, no. 3, pp. 1018–1037, 2012.

[16] Ningning Zhao, Qi Wei, Adrian Basarab, Denis Kouamé, and Jean-Yves Tourneret, "Blind deconvolution of medical ultrasound images using a parametric model for the point spread function," in *Ultrasonics Symposium (IUS), 2016 IEEE International*. IEEE, 2016, pp. 1–4.

[17] Nico Vervliet, Otto Debals, Laurent Sorber, Marc Van Barel, and Lieven De Lathauwer, "Tensorlab 3.0," Mar. 2016, Available online.

[18] Alain Hore and Djemel Ziou, "Image quality metrics: Psnr vs. ssim," in *Pattern recognition (icpr), 2010 20th international conference on*. IEEE, 2010, pp. 2366–2369.